Synthesis and Rheology of Tailored Poly(dimethylsiloxane) Zinc and Sodium Ionomers

Ashish Batra, Claude Cohen,* and T. M. Duncan

School of Chemical and Biomolecular Engineering, Olin Hall, Cornell University, Ithaca, New York 14853

Received June 30, 2005; Revised Manuscript Received October 10, 2005

ABSTRACT: We describe a synthesis scheme for the preparation of "model" poly(dimethylsiloxane) ionomers with tailored number of monomers between ions and number of ions per chain. Melts of low ion concentration (0.3−1.3 mol %) model zinc and cobalt ionomers, and their unneutralized COOH precursors are found to precipitate as polymers that flow and exhibit a zero-shear viscosity but equilibrate to physical gels. The gel time follows an Arrhenius relationship and is used to predict and verify physical gel formation at room temperature over a time scale from several months to years. The gel time depends chiefly on the ion concentration (calculated here as the average number of ions per monomer units (×100)) and functionality (defined as the average number of ions per chain); for ionomers with comparable overall molar mass, the ion concentration and functionality act counter to each other. Unlike traditional hydrocarbon ionomers, gel formation in these polysiloxane ionomers is favored by high temperature, and the gel moduli are comparable to moduli of end-linked PDMS networks. We propose this is due to transformation of intramolecular interactions to intermolecular interactions at high temperatures. Sodium ionomers form critical gels immediately after precipitation which we attribute to the more ionic nature of sodium relative to the transition-metal ionomers.

1. Introduction

Ionomers are polymers with a low ion concentration (typically less than 15 mol %) of ionic groups covalently bound to a polymer backbone.[1] Most studies have focused on random copolymer ionomers or model telechelic ionomers.[1] Random copolymer ionomers (of ethylene or styrene with acrylic acid or methacrylic acid) lack the well-defined architecture necessary to characterize structure−property relationships.[2] Model telechelic ionomers have ionic groups located at one or both ends of the polymer chain. Extensive studies on telechelic ionomers have been reported by Jérôme and others,[3−6] but the influence of overall molar mass of the chain and ion concentration on rheology and morphology cannot be studied independently with these systems. The additional variable of functionality was introduced in model three-arm star ionomers of polyisobutylene with ionic groups at ends of the star arms.[7,8] Unlike high molar mass telechelics that would undergo chain extension due to ionic aggregate formation and result in highly entangled melts, these stars could form cross-linked networks in which the ionic aggregates act as weak cross-links.

The regular placement of ionic groups along a polymer chain usually requires a difficult and complicated synthesis. Ionenes (polymers prepared by quaternization of di-t-amines with dihalides) and block copolymer ionomers are examples of polymers with regular placement of ions along the backbone.[9] A series of papers by Cooper et al.[10−13] in the late 1980s and 1990s was devoted to model polyurethane ionomers in which the number of monomers between ions could be controlled. These model ionomers are synthesized as 1:1 copolymers of a diisocyanate and a macroglycol without a chain extender. Ionization of the urethane linkage precisely controls the placement of the ions. Ion concentration is typically in the range of 1.5−6 mol % for these studies.

Here, we synthesize similar model ionomers with tailored number of monomers between ions and number of ions per chain on a polysiloxane backbone. From a technological standpoint polysiloxanes have unique properties like thermal and oxidative stability, excellent dielectric properties, physiological inertness, and moisture resistance.[14] From a fundamental science standpoint, extensive literature[15−17] on model poly(dimethylsiloxane) (PDMS) networks allows us to compare directly mechanical properties of physical gels obtained from PDMS ionomers and networks obtained from end-linking PDMS. Moreover, the backbone flexibility, the very low glass temperature, and the interaction of ions with oxygen atoms on the backbone can lead to rheology and morphology of PDMS ionomers different than what has been observed with similar polyurethane or hydrocarbon-based model systems. Thus, PDMS is a promising material for making model ionomers.

Furthermore, we focus on melts of very low ion concentration ionomers (0.3−1.3 mol %) of zinc, cobalt, and sodium with emphasis on gelation. We will study the differences between the rheology of the transition-metal ionomers vs sodium ionomers.

Three schemes have been reported for synthesis of PDMS precursor chains containing side ionic groups: (1) direct modification of polysiloxane backbone, (2) ring-opening polymerization of functional cyclosiloxanes, and (3) polycondensation of bisilafunctional monomers.[18] One of the most popular and simple schemes for direct modification of the polysiloxane backbone involves hydrosilylation. Hydrosilylation is the catalyzed addition of Si−H to unsaturated compounds bearing functional groups such as carboxyl,[19] hydroxyl,[20] crown ether,[21] and acrylic.[22] All these functional groups can be converted to ionic groups on a poly(dimethyl-*co*-methylhydrosiloxane) backbone in the presence of a platinum catalyst. This scheme suffers from two drawbacks. First, the copolymer is usually a random copolymer and hence does not provide control over the number of monomers between ions. Second, end groups need to be unreactive because these are susceptible to side reactions during hydrosilylation. Polysiloxanes produced via this scheme are reviewed in detail by Boutevin et al.[18] We desire, however, a carboxyl-containing polysiloxane that has vinyl-terminated

10.1021/ma051418q CCC: $33.50
Published on Web 11/23/2005

chains, so that ends can be covalently linked to obtain end-linked ionomer networks.

Cationic or anionic ring-opening copolymerization of cyclic siloxane oligomers bearing functional groups can also produce linear polysiloxanes with pendent ionic groups. These schemes often result in high molecular weight but again suffer from random arrangement of ions.[23−29]

Hydrolytic polycondensation to produce homopolymers consists of an acid- or base-catalyzed hydrolysis that converts difunctional monomers into cyclic oligomers, which are subsequently polymerized in the presence of ionic catalysts.[30−33] One advantage of such schemes is that the polymer has hydroxyl-terminated chains and hence can be further converted to vinyl-terminated chains and eventually cross-linked.

But, heterofunctional polycondensation is the most efficient scheme to incorporate pendent carboxyl groups at regular intervals. This scheme relies on the ability of the silanol group to react with various silicon functional groups to produce the siloxane linkage. The silicon functional groups most often used for this purpose are the following: −Si−Cl, −Si−O−COR, −Si−OR, −Si−NR, and Si−H.[18] Klok et al.[34] have used this scheme with commercially available hydroxyl-terminated PDMS and a *tert*-butylcarboxylate-functionalized dichlorosilane followed by thermal cleavage of the ester bond. We will use a similar synthesis scheme outlined below. This scheme allows regular placement of the carboxyl group and vinyl-terminated chains.

2. Experimental Procedures

2.1. Synthesis of "Model" Poly(dimethylsiloxane) with Interacting Groups. The synthesis scheme is simple in concept; polycondensation of hydroxyl-terminated PDMS of low polydispersity with a dichlorosilane compound containing a protected carboxylic acid group incorporates a carboxyl group at fixed intervals. The interval is determined by the molar mass of OH-PDMS-OH. The amount of the dichlorosilane compound added to the reaction mixture controls the average degree of polycondensation and thus controls the number of carboxyl groups per chain. The final step after removal of the protecting group is a fractionation in a good/bad solvent mixture to yield fractions with low polydispersity. The synthesis scheme is executed in five steps.

Step one is the synthesis of low-polydispersity hydroxyl-terminated PDMS chains. These were synthesized from hexamethylcyclotrisiloxane (D_3) monomer (Gelest, Inc.) by anionic ring-opening polymerization in a 50 wt % toluene solution at 60 °C catalyzed by benzyltrimethylammoniumbis(*o*-phenylenedioxy)-phenylsiliconate) and promoted by dimethyl sulfoxide (DMSO). Calculated amounts of water[35] were added to control the molecular weight of the resulting polymer. The polymer samples thus obtained were washed with water, dissolved in toluene, reprecipitated with toluene and methanol, and then dried in a vacuum oven at 60 °C for 3 days. The details of the catalyst preparation and polymer synthesis have been reported elsewhere.[15,35−37] These precursor chains were characterized using gel permeation chromatography (GPC) to measure the polystyrene-equivalent number-average molar mass and polydispersity index (PDI). A correction to the molar masses based on an established calibration curve for PDMS[15] was only 5% for the lowest molar mass precursor chain (6K) and much smaller for the higher molar mass ionomers. The GPC equipment consisted of a Waters model 6000A solvent delivery system, Waters Styragel columns HR 3 and HR 4 (with effective molar mass range of 500−30 000 and 5000−600 000 g/mol, respectively) calibrated with polystyrene standards from Scientific Polymer Products, Inc., and a Waters model R401 refractive index detector. Toluene was used as the solvent. Table 1 shows the polystyrene-equivalent molar mass (M_n), the molar mass corresponding to the peak position of the gel permeation chromatograph (M_{peak}), and PDI of the OH-PDMS-OH precursors. The precursor names are rounded-off values of M_{peak}.

Table 1. Molar Mass and Polydispersity of OH-Terminated PDMS Precursors Used for Synthesis

precursor chains	M_n (kg/mol)	M_{peak} (kg/mol)	PDI
6K	6.0	5.6	1.28
7K	6.5	6.7	1.22
8K	8.6	8.5	1.32
9K	9.3	9.1	1.32
11K	12.5	11.2	1.32
15K	16.4	14.7	1.37
18Ka	17.8	18.0	1.32
18Kb	19.6	18.1	1.40
24K	26.5	23.7	1.40
27K	29.5	27.2	1.32

Step two is the synthesis of a dichlorosilane compound containing a protected carboxylic acid group. Methyldichlorosilane is hydrosilylated (a Si−H group adds to a carbon−carbon double bond) with *tert*-butyl acrylate in the presence of a catalyst, *cis*-dichlorobis-(diethyl sulfide)platinum(II), at 45 °C. A small amount of 4-OH-TEMPO[38] was added to prevent the polymerization of *tert*-butyl acrylate. The progress of the reaction is tracked with ^{1}H NMR by monitoring the disappearance of the vinyl hydrogen atoms (typical time 4 days). The reaction flask was connected to a short-path distillation apparatus in turn connected to a dry receiver. A vacuum induced at room temperature removed excess dichlorosilane. Following this, the reaction flask was placed in an oil bath at 70 °C, and a colorless product was distilled under reduced pressure (∼30 in.Hg). The product was a mixture of the anti-Markovnikov and Markovnikov addition products (Figure 1). ^{1}H NMR in $CDCl_3$ of the mixture showed chemical shifts (in ppm) for the anti-Markonikov product at CH_3Si≡ 0.78 (s), ≡Si−CH_2− 1.42 (t), ≡Si−CH$_2$−CH_2− 2.4 (t), and −CH$_2$−COOC(CH_3)$_3$ 1.42 (s) and for the Markonikov product at CH_3Si≡ 0.85 (s), ≡Si−CH(CH$_3$)− 2.38 (q), ≡Si−CH(CH_3)− 1.28 (d), and −CH(CH$_3$)−COOC(CH_3)$_3$ 1.42 (s).

Step three is the synthesis of polymer chains by polycondensation of precursor PDMS chains and the dichlorosilane compound. To a 10 wt % solution of the OH-terminated PDMS in toluene, a 20% excess of the small molecule dissolved in toluene is added at a very slow rate using a syringe pump. The reaction mixture also contains 1 wt % pyridine that acts as an acid scavenger for the HCl released during the polycondensation. Very slow addition yields a higher degree of polycondensation as compared to fast addition. For higher molecular weight precursors, multiple additions are needed for an appreciable degree of polycondensation. For low molecular weight PDMS precursors (5−10 kg/mol), the average degree of polycondensation is from 7 to 10, whereas for higher molecular weights (15−30 kg/mol), the average degree of polycondensation is from 3 to 5. After the desired degree of polycondensation has been achieved, the end-capper vinyldimethylchlorosilane is added to terminate the OH chains with vinyl groups. The polymer solution is then washed with water and dried using crushed calcium hydride. The solution is then filtered and re-end-capped so that any chlorine end groups converted to hydroxyl groups after the water wash are now terminated with the vinyl groups. The polymer is washed with water and then precipitated in methanol and dried in a vacuum oven at 60 °C for 3 days. The ^{1}H NMR chemical shifts in $CDCl_3$ for the polycondensed polymer product are CH_3Si≡ 0.05 (s), ≡Si−CH_2− 0.82 (t), ≡Si−CH$_2$−CH_2− 2.4 (t), and −CH$_2$−COOC(CH_3)$_3$ 1.45 (s) (made from anti-Markonikov small molecule) and for the Markonikov product are CH_3Si≡ 0.05 (s), ≡Si−CH(CH$_3$)− 2.01 (q), ≡Si−CH−(CH_3)− 1.22 (d), and −CH$_2$−COOC(CH_3)$_3$ 1.45 (s).

Step four is deprotection, i.e., cleavage of the *tert*-butyl group. This is the most difficult step in the synthesis because of two issues. One, the PDMS backbone can break as well as rearrange in the presence of reagents typically used for deprotection. Acids such as trifluoroacetic acid,[39] formic acid,[40] *p*-toluenesulfonic acid,[41] and nitric acid[42] can break backbone chains if used in high concentra-

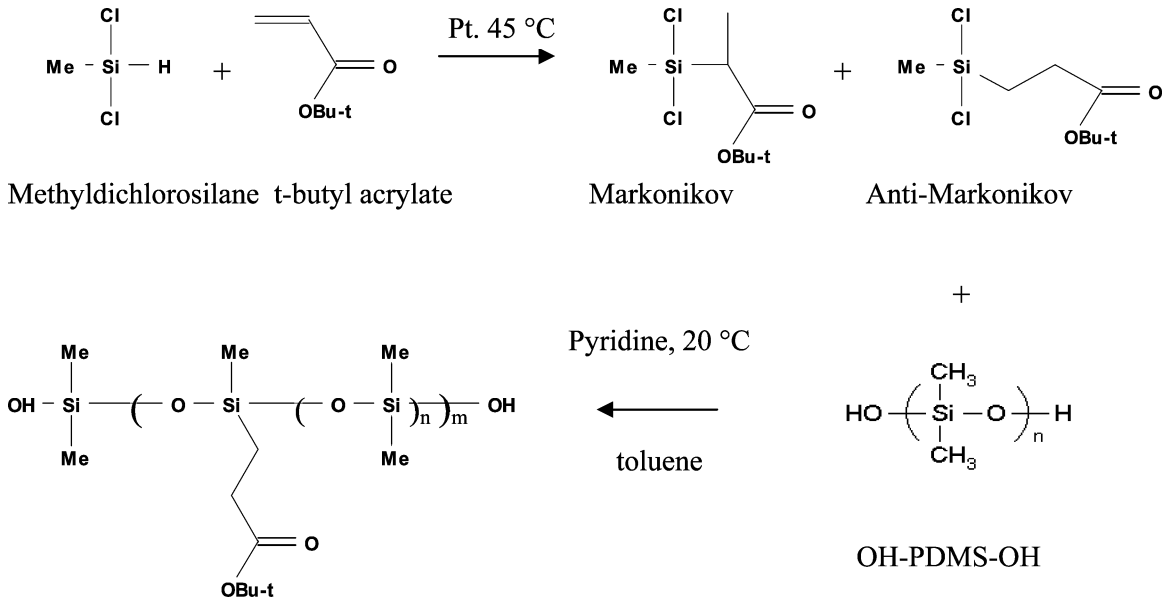

Figure 1. Steps two and three of the reaction scheme to prepare a polycondensed polysiloxane with *tert*-butyl groups at regular intervals.

tions to ensure 100% deprotection. Second, the hydrophobic nature of the siloxane backbone prevents use of some schemes used for small molecule deprotection. *tert*-Butyl groups can also be thermally cleaved by heating around 200 °C as demonstrated by Klok et al.,[34] but this scheme results in a gel-like material. Also, as we will show, thermal history is an important component to studying ionomers and therefore reactions in the melt at high temperatures must be avoided. Here we rely on a scheme proposed by Bindl et al.,[19] who found that acids such as triflic acid if used in ppm concentrations catalyze cleavage of *tert*-butyl groups which allows lower temperatures. We add ppm concentrations of triflic acid to a 10 wt % solution of the polycondensed product in toluene and heat the solution to 120 °C. Such low quantities of triflic acid act as a catalyst to reduce the temperature of thermal cleavage of the *tert*-butyl groups from 210 to 105 °C. Extreme care has to been taken in adding just the right quantity. Too much triflic acid can break the PDMS backbone, and too little does not cleave the *tert*-butyl groups. Just the right amount cleaves the *tert*-butyl completely but breaks some unreacted PDMS precursors, resulting in a long tail seen in the gel permeation chromatograph.

The required concentration of triflic acid is found empirically to be in the range of 2−3 μL/10 g of polycondensed polymer. Triflic acid acquires a yellowish tinge with age that reduces the efficacy of the acid and changes the concentration needed for complete deprotection. The peak position and most of the gel permeation chromatograph do not change between the polycondensed sample and the deprotected sample, implying that the polycondensed backbone remains intact and it is indeed the low molar mass PDMS precursors that break. It has been pointed out that the presence of strongly interacting groups can complicate characterization of molecular weights using GPC.[43] However, for the small mol % of interacting groups in the system considered, this is not the case.

In step five triflic acid is neutralized with sodium bicarbonate. Complete deprotection is verified using FTIR and NMR. In the NMR spectrum, the *tert*-butyl peak at 1.45 ppm disappears, and in the IR spectrum the stretching vibration of the *tert*-butyl carboxyl band at 1723 cm^{-1} shifts to the hydrogen-bonded acid band at 1713 cm^{-1}, as shown in Figure 2a. The deprotected polymer solution is passed through a syringe filter to remove the sodium bicarbonate. For samples to be studied in the acid form (hereafter called PDMS-COOH samples), the toluene solution of PDMS-COOH is further diluted to 2.5 wt % and then fractionated with methanol to yield narrower polydispersity fractions (1.3−1.6), as measured by GPC. To make ionomers, the PDMS-COOH solution obtained after filtration of sodium bicarbonate is first diluted to a 5 wt % solution in toluene, a 100% excess of zinc(II), sodium, or cobalt(II)

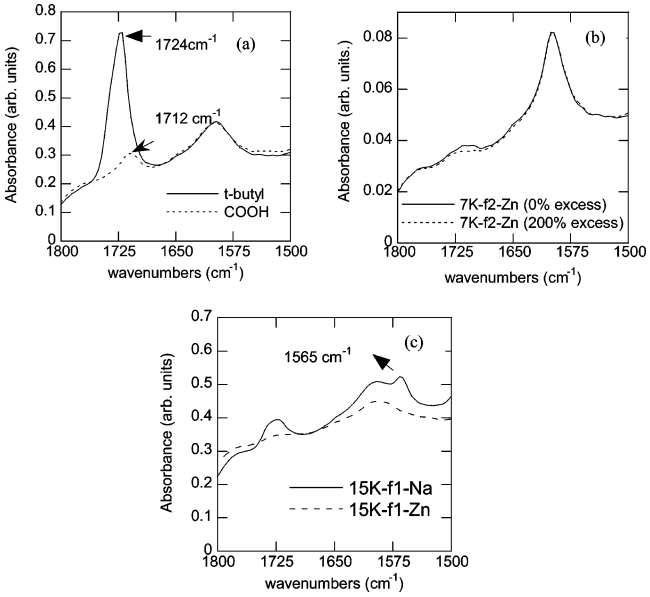

Figure 2. FTIR of (a) *tert*-butyl vs deprotected polymer, (b) 7K-f2-Zn (0% excess) vs 7K-f2-Zn (200% excess), and (c) 15K-f1-Zn vs 15K-f1-Na.

acetylacetonate (Aldrich) is added to the solution, and the slurry is allowed to stir vigorously at room temperature for a day. The solution is then filtered to remove excess salt and further diluted to a 2.5 wt % solution. Finally, fractionation with methanol yields narrow-polydispersity fractions.

Table 2 lists the ionomers used in this study with their M_n, molar masses corresponding to peak position (M_{peak}), PDI, the average number of COO$^-$ groups per chain (functionality), and ion concentration (calculated as the average number of ions per monomer units (×100) and expressed in mol %). The values of M_{peak} listed in Tables 1 and 2 are introduced to give additional information on the molar mass distribution. (For example, the percent difference between M_n and M_{peak} is quite small for the precursor chains but much larger for the fractionated ionomer chains despite comparable PDIs.) We also found it more convenient to define the number of ions per chain based on the peak molar mass (see below) so that an ionomer that leads to a physically cross-linked network would have an average of at least two ions per chain based on this definition. The average number of COO$^-$ groups per

Table 2. Molar Mass and Polydispersity of the Polymers Used in This Study

polymer chains (precursor-fraction-ion)	M_n (kg/mol)	M_{peak} (kg/mol)	PDI	no. of COO^- groups per chain (functionality)	ion concentration (mol %)
		Zinc Samples			
6K-f1-Zn	80.7	122.0	1.48	19	1.23
6K-f2-Zn	46.4	61.7	1.41	9	1.23
6K-f3-Zn	33.5	43.8	1.33	6	1.23
6K-f4-Zn	22.8	30.1	1.23	4	1.23
7K-f1-Zn	56.1	83.8	1.54	11	1.06
7K-f2-Zn	38.9	50.3	1.49	6	1.06
9K-f1-Zn	36.0	53.8	1.63	5	0.82
9K-f2-Zn	29.0	35.7	1.49	3	0.82
9K-f3-Zn	19.6	23.7	1.42	2	0.82
11K-f1-Zn	53.8	81.0	1.63	6	0.67
15K-f1-Zn	54.2	86.0	1.44	5	0.49
18Ka-f1-Zn	72.0	122.0	1.53	6	0.41
18Ka-f2-Zn	64.1	83.8	1.30	4	0.41
18Ka-f3-Zn	45.0	63.8	1.32	3	0.41
24K-f1-Zn	65.7	106.0	1.45	4	0.31
24K-f2-Zn	41.8	61.7	1.40	2	0.31
27K-f1-Zn	57.6	75.7	1.43	2	0.27
		Sodium Samples			
11K-f1-Na	61.3	81.0	1.51	6	0.67
11K-f2-Na	29.1	41.0	1.48	3	0.67
15K-f1-Na	55.0	81.0	1.50	4	0.49
18Kb-f1-Na	56.0	61.7	1.40	2	0.41
		COOH Samples			
11K-f1-H	60.0	81.0	1.58	6	0.67
27K-f1-H	61.7	86.7	1.51	2	0.27
		Unmodified PDMS			
reference	55.5	89.7	1.56	0	0
		Cobalt Samples			
7K-f1-Co	50.0	66.0	1.64	8	1.06
8K-f1-Co	43.0	57.0	1.59	6	0.93

chain is calculated as $\{(M_{peak}/M_n$ of precursor PDMS$) - 1\}$ with the assumption that there are no COO^- groups at the ends. However, if a fraction of chains have COO^- groups at both ends, the average number of COO^- groups is $\{(M_{peak}/M_n$ of precursor PDMS$) + 1\}$. For consistency, we assumed there are no COO^- end groups to characterize the ionomers used here. As an example of the nomenclature used in the paper, 6K−f1-Zn indicates 6K precursor chains, fraction 1, and counterion Zn.

In the FTIR spectra of ionomers, complete neutralization eliminates the band at 1712 cm^{-1}. This band is replaced by the asymmetric vibrations of the metal carboxylate in the 1500−1600 cm^{-1} range. For zinc ionomers of ethylene-*co*-methacrylic acid, Brozoski et al.[44] assigned the singlet band at 1585 cm^{-1} to the asymmetric carboxylate stretching vibration of a tetrahedral structure of the tetracoordinated zinc carboxylate multiplet. This is close to a band at 1600 cm^{-1} seen in unmodified PDMS and hence difficult to resolve separately. Figure 2b shows a low-intensity band at 1712 cm^{-1} if neutralization is carried out with a stoichiometric amount of zinc acetylacetonate, but this band disappears completely in the samples with 100% excess and 200% excess fractionated samples. For sodium PDMS ionomers, the asymmetric carboxylate stretching band appears at 1565 cm^{-1}, as shown in Figure 2c. Brozoski et al.[44] observed doublets at 1568/1547 cm^{-1} for sodium ionomers of ethylene−methacrylic acid. On exposure to water these are replaced by a singlet at 1540 cm^{-1} and a new band at 1700 cm^{-1} assigned to the acid group formed by exchange of sodium ions with protons in water.[45]

2.2. Rheology. Dynamic frequency sweeps were carried out with a Rheometrics RDA II rheometer in parallel plate geometry with 10 mm diameter plates to characterize the storage moduli, loss moduli, and complex viscosities as a function of annealing time at different temperatures.

3. Results and Discussion

3.1. Rheology and Gelation Properties of Zinc Ionomers. 3.1.1. Rheology of Fractionated Samples. Parts a, b, and c of Figure 3 show the rheology of zinc ionomer samples 7K-f1-Zn, 15K-f1-Zn, and 27K-f1-Zn, respectively, 1 day after their fractionation and drying at 50 °C to remove excess toluene or methanol. All samples precipitate as polymers with a moderate zero-shear viscosity. However, their rheology shows a marked difference from the rheology (in the same frequency range) of an unmodified PDMS sample (reference sample) of comparable molar mass and polydispersity shown in Figure 3d. If there are too few ions per chain, as in 27K-f1-Zn, then the zero-shear viscosity (30 Pa·s) is just twice that of the unmodified PDMS reference (15 Pa·s), and in the frequency range (1−100 rad/s) the storage modulus (G') is proportional to $\omega^{1.8}$ and the loss moduli (G'') is proportional to ω. If the number of ions per chain is large such as in 7K-f1-Zn, which has 11 COO^- sites per chain, a large deviation from the unmodified PDMS meltlike behavior is observed. The zero-shear viscosity is 100 times greater than that of the reference. But these freshly prepared samples are in a nonequilibrium state manifested 2 days after precipitation by a 2−3-fold increase in viscosity for samples with a moderate number of ions per chain (greater than 3). The viscosity continues to increase thereafter. Figure 4 shows the difference in rheology of the 15K-f1-Zn sample between day 1 and day 2.

3.1.2. Effect of Temperature on the Rheology of Fractionated Samples. Samples of 9K-f1-Zn were loaded on the rheometer 1 week after precipitation and warmed to a fixed temperature between 25 and 125 °C. Each sample was allowed to equilibrate at an elevated temperature for 0.5 h, before the dynamic frequency sweep was conducted. The storage modulus, loss modulus, and complex viscosity all decreased from their value at 25 °C when the equilibration temperature was varied from 25 to 100 °C. This is to be expected due to increased thermal motion; however, they all increased dramatically at 125 °C. After 0.5 h at 125 °C, G', G'', and η^* all followed a power law.[46] We interpret this to indicate the formation of a critical gel due to formation of physical cross-links, which could be single tetracoordinated zinc carboxylate triplets consisting of one zinc ion and two carboxylate ions belonging to different polymer chains or ionic triplets aggregated due to electrostatic interactions. In polysiloxanes, an additional interaction between oxygen atoms on the siloxane backbone and zinc atoms is also possible. The structure and morphology of these gels are discussed below.

3.1.3. Formation of Critical Gels. The gel time is the time at which the weight-average molar mass diverges to infinity or the largest cluster extends throughout the entire sample.[47] A critical gel forms at the gel time, and the stress relaxation moduli $G(t)$, G', and G'' show the following power law behavior:

$$G(t) = St^{-n} \qquad \lambda_0 < t < \infty \tag{1}$$

and

$$G' \sim G'' \sim \omega^n \qquad 0 < \omega < 1/\lambda_0 \tag{2}$$

The gel strength S and relaxation exponent n define the critical gel. The characteristic time λ_0 represents a lower cutoff due to glassy behavior at short time scales or at high frequencies. For physically cross-linked systems the finite lifetime (λ_1) of physical junctions limits the frequency range to the lower cutoff

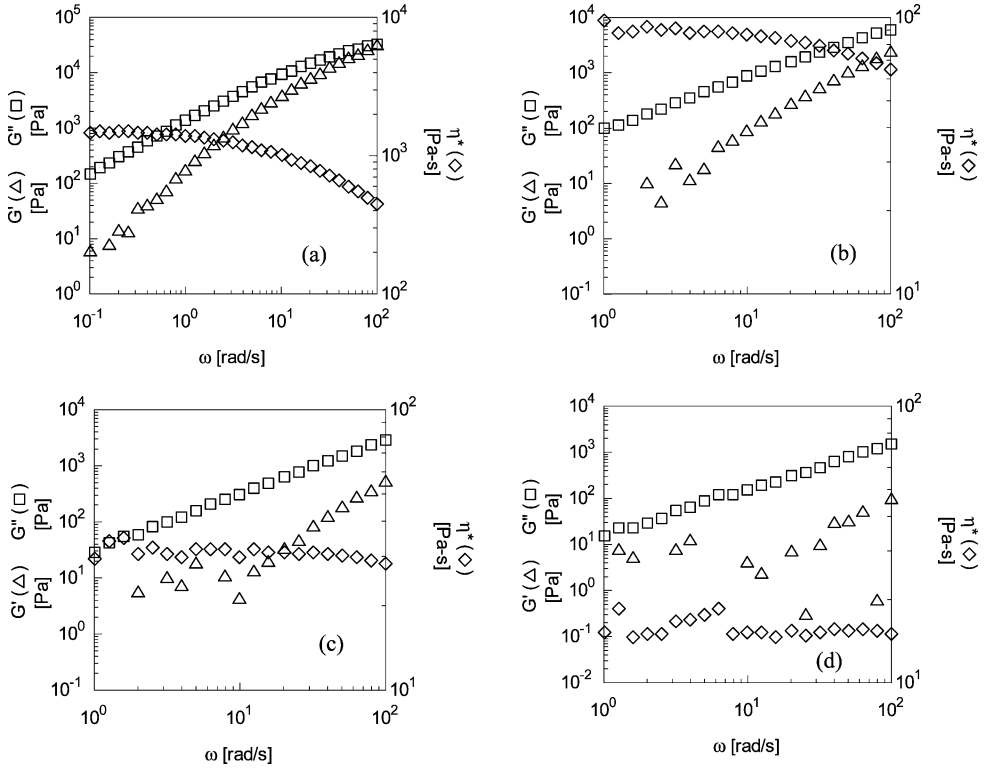

Figure 3. Storage modulus (G'), loss modulus (G''), and complex viscosity (η^*) at 25 °C of (a) 7K-f1-Zn, (b) 15K-f1-Zn, (c) 27K-f1-Zn, and (d) reference sample. All were measured 1 day after precipitation and drying.

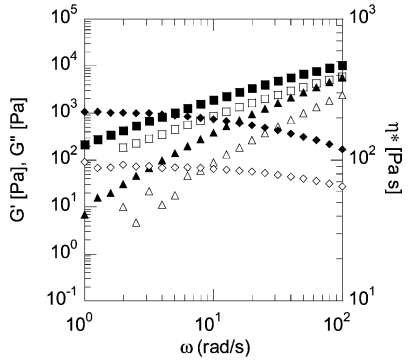

Figure 4. Rheology of 15K-f1-Zn at 25 °C 1 day after precipitation and drying (□, G''; △, G'; ◇, η^*) and 2 days after precipitation (■, G''; ▲, G'; ◆, η^*).

$1/\lambda_1$ such that in oscillatory shear for physical gels at the gel time the dynamic moduli scale with frequency as[48]

$$G' = \frac{G''}{\tan\delta} = S\Gamma(1-n)\cos\left(\frac{n\pi}{2}\right)\omega^n \qquad 1/\lambda_1 < \omega < 1/\lambda_0 \tag{3}$$

where $\Gamma(n)$ is the gamma function. The power-law dynamics of the modulus leads to a loss tangent, $\tan\delta$, that is frequency independent at the gel time and is a convenient experimental observable because at the gel time:

$$\tan\delta = \frac{G''}{G'} = \tan\left(\frac{n\pi}{2}\right) = \text{constant} \quad 1/\lambda_1 < \omega < 1/\lambda_0 \tag{4}$$

In addition, Te Nijenhuis and Winter[49] have also shown that plots of $\tan\delta$ vs time at various frequencies all intersect at the gel time. The gel formation observed after 0.5 h at 125 °C can be observed after longer annealing times at lower temperatures.

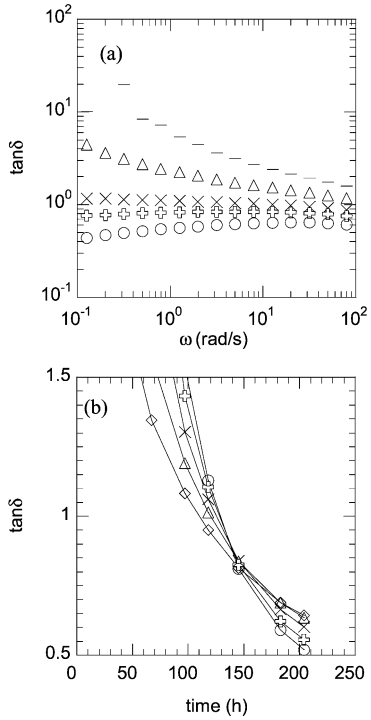

Figure 5. (a) Plot of tan δ vs frequency for several aging times for 9K-f1-Zn at 50 °C: (—) 31 h, (△) 67 h, (×) 118 h, (✣) 145 h, and (○) 204 h. (b) Plot of tan δ vs time at select frequencies: (◇) 31 rad/s, (△) 10 rad/s, (×) 3 rad/s, (✣) 1 rad/s, and (○) 0.5 rad/s.

Figure 5 shows the behavior of tan δ as a function of both frequency and time for the 9K-f1-Zn sample annealed at 50 °C. In Figure 5a, tan δ becomes independent of frequency at some time between 118 and 145 h, and in Figure 5b the curves intersect at 140 h. Thus, even at low temperatures, a critical

Table 3. Gel Times in hours for Zinc Ionomers at Various Temperatures

temp (°C)	6K-f1-Zn	6K-f2-Zn	9K-f1-Zn	9K-f2-Zn	18Ka-f1-Zn	18Ka-f2-Zn	24K-f1-Zn	27K-f1-Zn
75	34.0	69.0		34.0	230.5	284+	25.2	
100	5.3	14.5	2.0	5.5	28+	47	4.5	
125	2.0	2.7	0.4	1.25	5.25	9	0.75	4.5
150	0.5	0.8	0.12	0.55	1.1	2	0.25	0.75

Table 4. Activation Energy and Predicted Gel Time at 22 °C for Zinc Ionomers

sample	prefactor (10^{-11} h)	activation energy (kJ/mol)	predicted gel time at 295 K (months)
6K-f1-Zn	283.0	66.9	2.7
6K-f2-Zn	61.9	73.7	9.7
9K-f1-Zn	1.26	80.3	2.9
18Ka-f1-Zn	1.88	87.2	72.0
18Ka-f2-Zn	12.0	82.8	76.5
24K−f1-Zn	7.61	76.7	4.1

gel can form. In fact, we find that the gel time (t_{gel}) follows an Arrhenius behavior with respect to temperature given by

$$t_{gel} \sim \exp\left(\frac{E_a}{RT}\right) \tag{5}$$

where E_a is the apparent activation energy for gel formation, R is the gas constant, and T the temperature. Gel times vs inverse temperature of annealing for a few zinc ionomers are plotted in Figure 6, and the data are fit according to eq 5.

Table 3 lists the gel times of various zinc ionomers at temperatures between 75 and 150 °C, some of which are plotted in Figure 6. From Figure 6, the apparent activation energy of gelation can be determined from the slope of the Arrhenius behavior. Table 4 lists the prefactors, activation energies, and predicted gel times at 22 °C (based on prefactors and activation energy). No specific trends for the value of activation energy are found with regard to the ion concentration or functionality of the zinc ionomers. The range of apparent activation energy found here (67−87 kJ/mol) comprises values reported for other thermally activated gelation processes.[50−52] For comparison, the activation energies for segment level dynamics and for the bulk viscosity of PDMS were reported to be 27 and 15 kJ/mol, respectively.[53]

The gel times at 22 °C range from a few months to years. For 9K-f1-Zn, the gel time is predicted to be 2.9 months, and indeed as shown in Figure 7, the 9K-f1-Zn sample tested 3 months after precipitation exhibits critical gel behavior. As a comparison, Figure 7 also shows that 9K-f1-Zn heated to 150 °C for 2.5 h a few days after precipitation exhibits network formation well past the critical gel point.

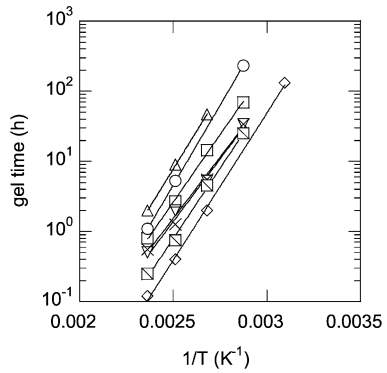

Figure 6. Gel time (t_{gel}) vs annealing temperature in Arrhenius representation for various zinc ionomers: (▽) 6K-f1-Zn, (□) 6K-f2-Zn, (◇) 9K-f1-Zn, (×) 9K-f2-Zn, (○) 18Ka-f1-Zn, (△) 18Ka-f2-Zn, (⧅) 24K-f1-Zn.

3.1.4. Effect of Temperature on Gel Time. The most striking feature of these zinc ionomers is the unusual decrease of gel time at higher temperatures. For typical hydrocarbon-based ionomers, thermal energy increases molecular motion and weakens a physical network at high temperatures; ultimately, the network flows at high temperatures. Ionomers are generally water-sensitive. Their rheological properties may be influenced by even ppm concentrations of water.[54] For the specific case of high mol % zinc ionomers derived from ethylene−methacrylic acid (E-MAA) the IR spectra remain unaffected in the presence of water, and there is no evidence of formation of acid salts or hydrogen-bonded dimers in the presence of water.[45] IR spectra show a peak at 1585 cm^{-1} which is interpreted as electrically neutral tetrahedrally coordinated zinc. Welty et al.[55] interpret extended X-ray absorption fine structure (EXAFS) spectra of fully dried E-MAA ionomers to indicate zinc coordinated to four oxygen atoms. The addition of water changes the EXAFS spectra, but the pattern was still characteristic of zinc coordinated to four oxygen atoms. Ishioka et al.[56] have also studied the IR and EXAFS of zinc ionomers of EMAA and concluded that in both wet and dry states the coordination number is four. On the basis of these observations, it would be reasonable to assume that zinc ions in PDMS ionomers remain largely tetracoordinated irrespective of water content.

The consistent trends of gel time vs temperature in Figure 6 cannot however be explained on the basis of random drying of water bound in these ionomers. Vasilev et al.[28] offer a more plausible explanation for the faster gel formation at high temperatures: the siloxane backbone unfolds from a spiral conformation, causing intramolecular interactions to convert to intermolecular interactions.[26] The insensitivity of the activation energy to the structure and molar mass of ionomers supports this explanation.

3.1.5. Characteristics of the Critical Gels. The values of the strength S and exponent n in eq 1 can reveal some information about the structure of the critical gels. The fractal dimension of a molecular cluster d_f is defined by

$$R \sim M^{1/d_f} \tag{6}$$

where R is the radius of gyration and M the molar mass of the cluster.[57] The fractal dimension at the gel time has been previously reported to be 4 independent of space dimensionality

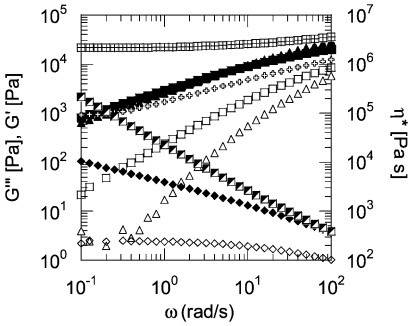

Figure 7. (□) G'', (△) G', and (◇) η^* for sample 9K-f1-Zn at 25 °C a few days after precipitation; (■) G'', (▲) G', and (◆) η^* taken 3 months after precipitation (critical gel); (⊞) G'', (⊞) G', and (◩) η^* heated to 150 °C for 2.5 h after a few days after precipitation.

Table 5. t_{gel}, n, S, and d_f for a Series of Constant Overall Molar Mass Zinc Ionomers

overall molar mass (kg/mol)	polymer chains	ion concn (mol %)	functionality	t_{gel} (h)	n	S (Pa·s^n)	d_f
60	18Ka-f3-Zn	0.41	3	9+			
	9K-f1-Zn	0.82	5	0.4	0.55	158	1.93
	6K-f2-Zn	1.23	9	2.7	0.48	519	2.02
80	27K-f1-Zn	0.27	2	4.5	0.48	784	2.02
	11K-f1-Zn	0.67	6	1.2	0.55	297	1.93
	7K-f1-Zn	1.06	11	10.5	0.54	5888	1.95
120	24K-f1-Zn	0.31	4	0.75	0.53	523	1.96
	18Ka-f1-Zn	0.41	6	5.25	0.34	5370	2.18
	6K-f1-Zn	1.23	19	2.0	0.47	4110	2.03

using the Zimm−Stockmayer theory of gelation, and a corresponding value of the relaxation exponent $n = 1$ was predicted.[58] Percolation theory predicts a value of d_f equal to 2.5 based on a space dimensionality of 3. In polymer systems where hydrodynamic interactions are completely screened but excluded-volume interactions dominate, n is expressed as[58]

$$n = \frac{d}{d_f + 2} \tag{7}$$

where d is the space dimension and d_f the fractal dimension. On the basis of eq 7, percolation theory ($d_f = 2.5$ and $d = 3$) would predict $n = {}^2/_3$, which is observed in many experimental systems.[50,59] If however the fractal dimension is between 1 and 3 and $d = 3$, then the exponent n will be between ${}^3/_5$ and 1. In polymer systems where excluded-volume effects as well as hydrodynamic interactions are completely screened, n is expressed as[58]

$$n = \frac{d(d + 2 - 2d_f)}{2(d + 2 - d_f)} \tag{8}$$

All values of n between 0 and 1 are possible for the physically acceptable range of d_f between 1 and 3.

For partial screening of excluded-volume interactions, values between those predicted by eq 7 and eq 8 will be obtained. For various physical gelation systems, a wide range of n and S with different correlations between n and S have been reported in the literature.[59−61] For many chemically cross-linked systems[62,63] S and n are related by

$$S = G_e\left(\frac{\eta_0}{G_e}\right)^n \tag{9}$$

where G_e represents the plateau modulus of the fully cross-linked material and η_0 represents the zero-shear viscosity of the precursor. However, the above expression and others relating S to temperature[48] were found to be invalid in physically cross-linked systems such as crystallizing polypropylene.[60]

In Table 5, we report the values of n, S, t_{gel}, and d_f (based on the assumption of complete screening of excluded-volume interactions, eq 8) for various samples at 125 °C. The value of n did not seem to depend on the temperature of gelation and has therefore been reported for a single temperature. The exponent n does not vary significantly, and the value of n is between 0.34 and 0.55 across all zinc samples. The value of S was found to decrease slightly with increase in temperature. Quantification of this trend was not possible due to lack of measurement at the exact gel point in some cases. For the same ion concentration samples such as 6K-f1-Zn and 6K-f2-Zn the value of n is lower and the value of S is higher for the higher molecular weight sample. This can also be interpreted as a decrease in n with increase in functionality because the first fractions always have more ions than the second fractions. No specific trends are observed with regard to whether the molar mass between ions is lower than entanglement molar mass or higher or high or low overall molar mass.

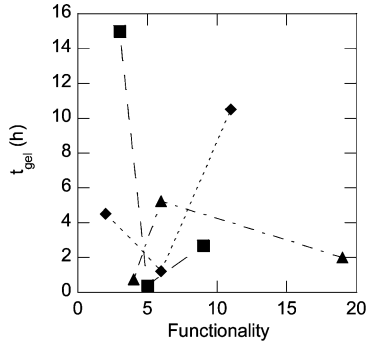

Figure 8. Gel time vs functionality for constant overall molar mass (■) 60K, (◆) 80K, and (▲) 120K.

Given the aforementioned diversity in relationship between n and S, it is not surprising that n and S do not follow a particular trend with regard to temperature or any other variable such as functionality, ion concentration, or overall molar mass for the ionomers considered here. The reason why the data have been arranged in sets for constant overall molar masses of 60K, 80K, and 120K (M_{peak}) in Table 5 will become clear in the following discussion of gel time dependence on the three inherent variables in our ionomer samples: (1) the functionality (number of ions per chain), (2) the ion concentration which is inversely related to the spacing between the ions, and (3) the overall molar mass.

3.1.6. Structural Parameters Affecting the Gel Time. For a discussion of gel time we first identify samples that have similar overall molar mass (within 10−20%) but have different functionalities and ion concentrations. We identify from Table 2 three such sets of samples. One with an overall molar mass of roughly 60K (based on peak position) consists of 18Ka-f3-Zn, 9K-f1-Zn, and 6K-f2-Zn. The second set with an overall molar mass of roughly 80K consists of 27K-f1-Zn, 11K-f1-Zn, and 7K-f1-Zn. The third set with an overall molar mass of roughly 120K consists of 24K-f1-Zn, 18Ka-f1-Zn, and 6K-f1-Zn. The values of the critical gel parameters n and S, the gel time (t_{gel}), and the fractal dimension of the critical gels (d_f) based on eq 8 are listed in Table 5 for these sets of similar molar mass ionomers. At a constant overall molar mass, the functionality and ion concentration are directly related; an increase in functionality implies an increase in ion concentration.

In Figure 8, we plot the gel time vs functionality for the three sets of similar molar mass ionomers. We find a maximum in the gel time with increasing functionality (and hence increasing ion concentration) for the overall molar mass 120K and minima in the gel time for the overall molar mass 60K and 80K. To interpret this interesting result, we investigate the effect of ion concentration and of functionality, keeping one constant and varying the other with an associated change in molar mass.

We find that, for ionomers having the same functionality (such as 24K-f1-Zn and 18Ka-f2-Zn (with functionality ∼ 4) or 6K-f3-Zn and 9K-f1-Zn (with functionality ∼ 6)) but different ion concentration leading to slightly different molar mass (within 30% of each other), the gel time increases as the ion concentration increases (refer to Table 3). We take this result to imply that for a similar molar mass an increase in ion concentration leads to an increase in gel time. Because ion concentration is inversely related to the number of monomers between ions, at a higher ion concentration, the chain length between ions is

shorter. We speculate that due to the shorter chain length between ions, intramolecular interactions will be favored and these must first convert to intermolecular interactions to form a critical gel, which leads to longer gel times.

On the other hand, for ionomers with the same ion concentration but with different functionality (such as 9K-f2-Zn and 9K-f3-Zn or 6K-f2-Zn and 6K-f3-Zn) leading to slightly different molar mass, the gel time decreases as the functionality increases (refer to Table 3). For similar molar mass, we can then anticipate that the time to gel would decrease as functionality increases. This can be simply explained by an increase in the cross-link ionic sites available for physical gel formation due to interactions between ion pairs. The larger the number, the quicker the sample can get to a critical gel state.

For a constant molar mass, the two variables of ion concentration and functionality are not however independent because as functionality increases, so does ion concentration. But ion concentration and functionality have opposite effects on the gel time. Therefore, when ionomers with the same molar mass but with different functionality and ion concentration are considered, the gel time is subject to two competing influences: a higher functionality decreases the gel time, and a higher ion concentration increases the gel time. One can expect a maximum or a minimum in the gel time as found in our observations. For 80K at high ion concentration, the gel time is dominated by the ion concentration and starts at the upper right-hand corner in Figure 8. As the ion concentration decreases, the gel time decreases up to the point where the effect of functionality becomes dominant, and as the ion concentration decreases further, the gel time starts to increase. Similar arguments can be made for the high molar mass ionomer (120K), except that in this case the dominant effect at high ion concentration is the functionality and not the ion concentration.

It is interesting to note from Table 5 that for the 80K and 120K sets S seems to the follow the trend of a minimum and a maximum of t_{gel}, whereas n follows a mirror-image behavior, having a maximum when S has a minimum. This implies that the values of n and S are also subject to the competing influences of ion concentration and functionality which is why no simple monotonic trends in these values as a function of overall molar mass or functionality were observed. The value of the fractal dimension based on eq 8 is found to be very close 2.0 for all the samples considered.

If any of zinc ionomers above the critical gel state are put in a solution of a nonpolar solvent like toluene, they swell like a covalently cross-linked PDMS network. Reversibility in these networks is demonstrated by swelling in a 50:50 mixture of tetrahydrofuran (THF) and water. THF is a good solvent for PDMS and allows water to migrate to ionic triplets, breaking them up and dissolving the physical cross-linking. If an ionomer network with a low modulus, obtained for example by aging a low ion concentration sample for a few months at room temperature, is subjected to a THF:water solution, then the cross-linking is completely reversed and a polymer solution is obtained. If an ionomer network with high ion concentration and a high modulus, obtained, for example by heating it to 150 °C for several days, is subjected to a THF:water solution, it resists dissolution for months.

3.2. Morphology and Structure in Zinc Ionomers. Small-angle X-ray scattering and scanning transmission electron microscopy of these model systems as a function of the counterion will be presented in a future publication.[46,64] Here we mention the results relevant to the low mol % zinc ionomers. SAXS does not reveal an ionic scattering peak, the characteristic feature in SAXS of hydrocarbon-based ionomers.[65] This feature is missing from both the as-precipitated zinc samples and equilibrated samples that have been heated to 150 °C for 20 days. However, a scattering intensity upturn at low angles is observed for all zinc ionomers.

Scanning transmission electron microscopy (STEM) micrographs are featureless. We interpret this to imply the absence of aggregated ionic triplets in these equilibrated networks. Thus, lone tetrahedrally coordinated ion triplets of carboxylate anions and zinc are distributed throughout the equilibrated network. Barium ionomers with similar number of ions per chain, number of monomers between ions, and overall molar mass have STEM micrographs with fascinating morphologies of rodlike aggregates and bundles of rods.[46,64] Because the atomic numbers of sodium (11) and silicon (14) are similar, STEM micrographs of sodium ionomers cannot be resolved.

These observations indicate that as the network structure of zinc ionomers equilibrate zinc−carboxyl triplets do not form aggregates. Polymer chains dissociate and reorganize intramolecular interactions into intermolecular interactions to form networks. The activated process is faster at higher temperatures.

3.3. Effect of Method of Preparation. We note that throughout this study 100% excess salt was used to neutralize the PDMS-COOH precursor to ensure complete conversion. Other have pointed out that for materials neutralized in homogeneous solutions excess salt could be trapped in the ionic aggregates.[66] This in turn either tightens the ionic associations or accelerates flow by allowing ionic groups to hop as ion quartets rather than as ion pairs.[67] Both scenarios have been observed on the basis of the neutralizing salt used.[67] However, these effects dominate for low molar mass ionomers with high mole content of ions. For high molecular weight ionomers with 1−5 mol % of ions, 50% excess salt is recommended.[68] Vasil'ev et al.[28] have also shown using XPS that 100% excess of zinc acetate was needed to ensure complete neutralization.

The zero-shear viscosity of a 7K-f2-Zn sample neutralized by a stoichiometric quantity of zinc is 8 Pa·s compared to 12 Pa·s for a 7K-f2-Zn sample neutralized by 200% excess salt. This increase could be explained by the increase in the number of sites neutralized by zinc which act as effective cross-link sites. As shown in Figure 2b, the FTIR spectrum indeed shows a free acid peak at 1712 cm^{-1} for 7K-f2-Zn with 0% excess salt, indicating incomplete neutralization. Both these samples when heated to 150 °C form a critical gel as expected, but the gel time is 17 h for stoichiometric neutralized compared to 37 h for the 200% excess. This could be explained by an increase and strengthening of the intramolecular ionic associations at room temperature that take longer to convert to intermolecular associations. At the gel time both samples have similar n and S values ($n \sim 0.65-0.7$; $S = 154$ Pa·$s^{0.65}$ at 150 °C). We consistently used 100% excess for all zinc ionomers to allow direct comparisons between samples.

More dramatic differences are observed when instead of low-polydispersity samples obtained by fractionating the ionomer samples in a methanol/toluene solution, high-polydispersity samples are directly recovered by evaporation of toluene. These samples also form gels and show an ionic peak as well as an upturn in SAXS.[46,64] Moreover, Figure 9 shows that there is a marked difference in the IR spectra of evaporated samples vs the corresponding fractionated samples. Though the evaporated samples would retain the excess salt, the bands in the region 1500−1800 cm^{-1} in the IR spectra of the evaporated samples do not correspond solely to the contribution from the unbound salt. In the evaporated samples, bands at 1565 and 1535 cm^{-1}

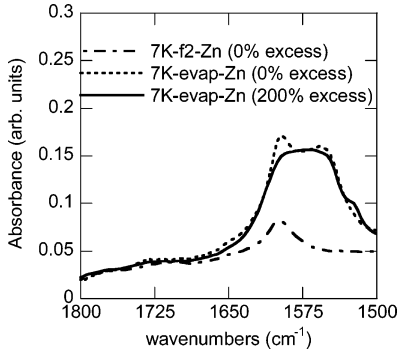

Figure 9. FTIR of zinc ionomers prepared by evaporation vs fractionation.

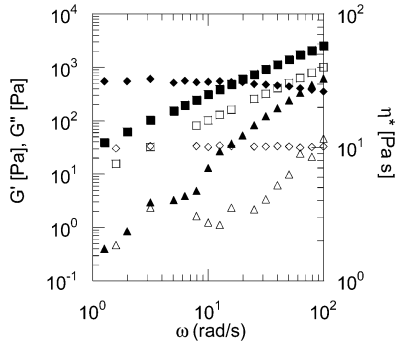

Figure 10. Rheology of 11K-f1-H at 25 °C 1 day after precipitation and drying (□, G''; △, G'; ◇, η^*) and 1 year after precipitation (■, G''; ▲, G'; ◆, η^*).

in Figure 9 can be identified. Coleman et al.[69] have assigned peaks in FTIR of E-MAA zinc ionomers at 1536 and 1565 cm^{-1} to a hexacoordinated zinc carboxylate mutiplet and also identified an acid salt structure which has bands at 1620 and 1537 cm^{-1}. Ishioka et al.[56] find, on the other hand, that a 1585 cm^{-1} band occurs only in the wet state whereas the triplet 1537, 1554, and 1625 cm^{-1} is observed in the dry state, and EXAFS does not show any evidence of a hexacoordinated zinc carboxylate. They argued that these differences can be attributed to reversible geometrical distortion of the tetrahedral coordination structure. However, Kutsumizu et al.[70] have also shown using IR that at 403 K increase in pressure on their ionomers shifts the peak from 1538 to 1585 cm^{-1} which they attributed to zinc structures changing from hexacoordinated to tetracoordinated. In the absence of a definitive technique to verify the increase in coordination number from 4 to 6 between the fractionated samples and the evaporated samples, we cannot say with certainty that the shifts in IR observed in these samples are indeed caused by this coordination number difference.

3.4. Properties and Gelation of PDMS-COOH Polymers. Figure 10 shows the rheological properties of 11K-f1-H 1 day and 1 year after precipitation. These properties immediately after precipitation do not deviate from the rheology of unmodified PDMS of comparable molar mass and polydispersity at room temperature. The nonequilibrium state of 11K-f1-H at room temperature is evident in the 2-fold increase in viscosity over a year. The much weaker interactions in the COOH samples as compared to those in the zinc ionomers are evident both by this extremely slow increase in viscosity and by a comparison of zero-shear viscosities a day after precipitation. 11K-f1-Zn has a zero-shear viscosity of 50 Pa·s whereas 11K-f1-H has a zero-shear viscosity of 15 Pa·s. The zero-shear viscosity of 27K-f1-Zn has a value of 30 Pa·s as compared to 16 Pa·s for 27K-f1-H. Heating these COOH samples initially decreases the viscosity similar to that observed with the ionomers as expected. Longer exposures of these samples to high temperatures, such as 125 °C, lead also to the formation of a critical gel and eventually a network.

The gel time for COOH samples also follows an Arrhenius behavior with an apparent activation energy (70 kJ/mol) similar to that of the corresponding zinc ionomer. However, the gel times for COOH systems are at least an order of magnitude longer than in comparable zinc ionomers. For example, at 125 °C 11K-f1-H forms a critical gel in 24 h compared to only 1.2 h for 11K-f1-Zn. This can be simply explained by the greater strength of ionic interactions compared to hydrogen-bond interactions. The Arrhenius behavior of 11K-f1-H, if extrapolated to room temperature, predicts 5.5 years for critical gel formation. It would take 6 months for the sample to gel at 50 °C, 24 days at 75 °C, and 5 days at 100 °C. Thus, for practical purposes, these COOH samples may be considered to be in a quasi-equilibrium state as viscous liquids for temperatures below 75 °C.

It should also be mentioned that if the number of COOH groups per chain is increased dramatically such as in the extreme case of replacing one methyl group on each silicon by a COOH group (poly(2-carboxyethylmethylsiloxane), a rubberlike latex with a milky color is obtained at room temperature.[30] Further, by forming a homogeneous blend of PDMS with poly(2-carboxyethylmethylsiloxane), Ohyanagi et al.[30] have concluded that hydrogen bonds form between the oxygen in PDMS with the COOH of poly(2-carboxyethylmethylsiloxane). On the basis of these results, it is fair to assume that in the systems considered here both intermolecular and intramolecular bonds between COOH groups and between the siloxane oxygen and COOH exist at room temperature.

High temperatures serve to convert most of the intramolecular bonds into intermolecular bonds, causing the formation of critical gels and eventually networks with frequency-independent G' at low frequencies. This rearrangement is the driving force for gel formation at higher temperatures as argued by Shchegolikina et al.[26] on the basis of the opening up of the spiral structure of PDMS at high temperatures. At moderate temperatures, viscosity decreases initially due to increased thermal motion because the unfolding process is still slow. However, at higher temperatures the unfolding process begins to dominate, which leads to large numbers of intermolecular bonds between COOH groups, which increases the viscosity with the eventual formation of a network. Klok et al.[34] and Rogovina et al.[27] point out that large aggregates of COOH akin to multiplets in ionomers might exist in these systems, but evidence for these using SAXS or STEM is not possible.

Rheology can be used to distinguish between the large domains and small domains of intermolecular bonded COOH groups only in extreme cases. Larger domains have a higher functionality of the cross-link point and in the extreme limit of infinite functionality would lead to a theoretical 2-fold increase in modulus compared to a tetrafunctional cross-link. For the systems considered here such extremes are unlikely. The extremely slow dynamics in our systems are attributed to the low COOH content. Once a large number of intermolecular bonds or aggregates of COOH groups have formed, the mobility of the chains decreases further. Using FTIR the formation of anhydrides has been ruled out by us as well as by others for similar systems.[35]

Vasilev et al.[71] have distinguished a few regimes of temperature in carboxyl-containing poly(dimethylcarbosiloxane)s. Our observations of critical gel times provide insights into those

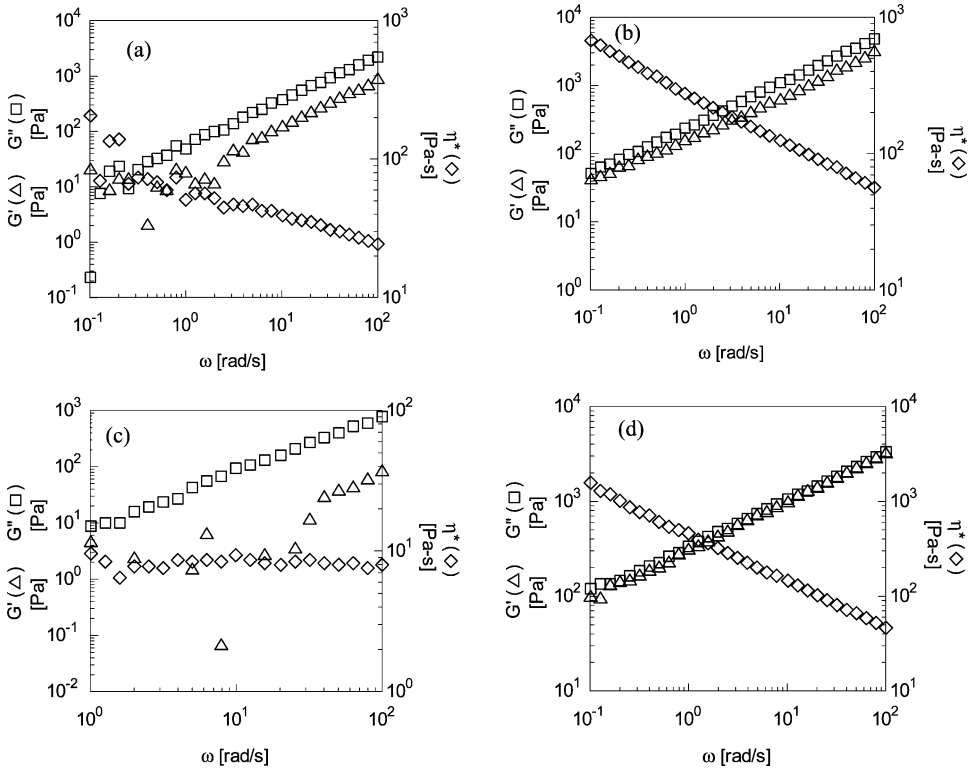

Figure 11. (a) G', G'', and η^* at 25 °C for 11K-f1-Na 1 day after precipitation and drying, (b) 14 days later (c) G', G'', and η^* at 25 °C for 11K-f2-Na 2 months after precipitation and drying (d) 11K-f2-Na at gel point after an hour of annealing at 125 °C.

regimes. The first temperature regime is below 50 °C and corresponds to critical gel formation on the order of years and samples are dominated by intramolecular hydrogen bonds. The second regime is the range of 50−100 °C and corresponds to critical gel formation on the order of weeks, and samples have more intermolecular bonds than in regime one. The third regime is the range of 100−175 °C and corresponds to critical gel formation on the order of hours, and samples are dominated by intermolecular bonds. Regime three yields three-dimensional networks that retain a significant fraction of intermolecular bonds on cooling. It is interesting to note that the value of exponent n of the critical gel (and hence the fractal dimension) of 11K-f1-H is approximately the same as for the 11K-f1-Zn, but the strength S has a lower value (at 125 °C $n = 0.54$ and $S = 148$ Pa·s$^{0.54}$ for 11K-f1-H as against $n = 0.55$ and $S = 297$ Pa·s$^{0.55}$ for 11K-f1-Zn).

3.5. Properties of Sodium Ionomers in Comparison to Zinc Ionomers. Figure 11a shows the rheology of the freshly precipitated 11K-f1-Na ionomer. It is evident that this sample precipitates as a weak critical gel with power law behavior of G' and G''. The sample 15K-f1-Na also shows this power law behavior 1 day after precipitation. Sample 11K-f1-Na has a n value of close to 1 (0.96) and a S value of 9.6 Pa·s$^{0.96}$. It is interesting to note that a similar zinc ionomer (11K-f1-Zn) would take months at room temperature to gel. The rheology of the 11K-f1-Na sample (shown in Figure 11b) 15 days after precipitation shows a much stronger gel state (higher modulus). On the basis of these results, it is reasonable to deduce that interactions are stronger in sodium ionomers. Sample 11K-f2-Na (shown in Figure 11c), however, does not show this critical gel behavior immediately after precipitation, and this can be attributed to the small (2−3) number of ions per chain. However, heating 11K-f2-Na to 125 °C for 10 h resulted in a critical gel being formed (Figure 11d) (with $n = 0.53$ and $S = 229$ Pa·s$^{0.53}$). A comparable zinc ionomer sample 9K-f2-Zn with three ions per chain forms a critical gel at 125 °C in only 1.25 h. This might at first seem a contradiction to the statement that sodium ionomers have stronger interactions, but because 9K-f2-Zn and 11K-f2-Na have limited ions per chain (3), in zinc ionomers a tetrahedral triplet involving two COO^- groups can act as a cross-link which leads to quick critical gel formation, whereas a lone sodium ion pair (sodium being monovalent) cannot act as a cross-link.

The difference in the flow properties between ionomers neutralized by different counterions such as zinc and sodium has been interpreted in terms of the charge to ionic radius ratio (q/a) of the cation,[72] ionic/covalent character of the cation,[73] its electronic configuration, and the stability constant of the neutralization reaction.[74] For transition metal ionomers, the carboxylate group is an electron donor (ligand) interacting with the metal cation, which is electron-deficient, whereas for alkali metals the interaction has a more ionic nature.[75,76] Two different structure formations have been proposed for these different types of ionomers: multiplet cluster structure for alkali metal ions like sodium and a coordinated complex structure for transition metals like zinc.[77]

3.6. Properties of Cobalt Ionomers in Comparison to Zinc Ionomers. Figure 12a,b shows that the rheology of ionomers 7K-f1-Co and 8K-f1-Co synthesized from cobalt(II) acetylacetonate is similar to zinc ionomers. These ionomers also precipitate with a zero-shear viscosity and evolve to a critical gel state. Similar to the case of zinc ionomers, STEM micrographs from cobalt ionomers are featureless. We interpret this to indicate the absence of any aggregates of cobalt−carboxyl triplets. In a subsequent paper[64] we will show that gallium and barium ionomers are similar to sodium in that they precipitate as gels above the critical gel state. These ionomers in contrast to zinc and cobalt ionomers form ionic aggregates.[64] These observations lead us to classify rheological behavior in terms

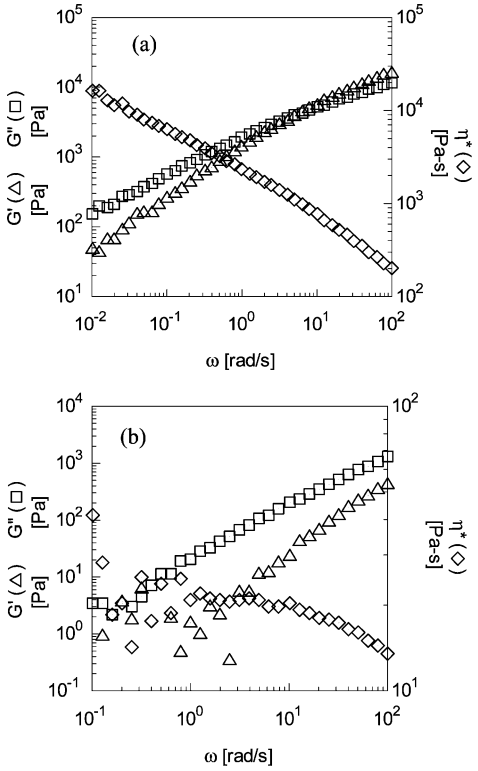

Figure 12. (a) G', G'', and η^* at 25 °C for 7K-f1-Co 2 weeks after precipitation and (b) 8K-f1-Co 1 day after precipitation.

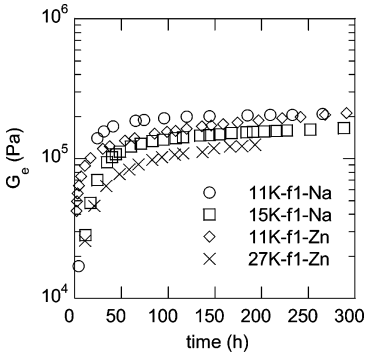

Figure 13. Evolution of the equilibrium modulus (G_e) at 150 °C.

of those of transition metal vs alkali and alkaline earth metal ionomers

3.7. Evolution of the Equilibrium Network State. All ionomers considered in this study precipitate in a nonequilibrium state at room temperature. They precipitate either as samples that flow and have a zero-shear viscosity, such as in zinc and cobalt ionomers and their COOH precursors, or as samples that precipitate as soft critical gels, such as sodium ionomers. However, heating at high temperatures or waiting at lower temperature results in a critical gel and eventually a permanent network. To determine the equilibrium state of the samples, we followed the evolution of the elastic modulus at 150 °C, as shown in Figure 13. The elastic modulus was approximated as the value of the storage modulus at 0.1 rad/s. This is a reasonable approximation for annealing times greater than 24 h as the storage modulus becomes practically independent of frequency below 0.1 rad/s. For annealing times less than 24 h, the modulus is changing faster than the time taken for storage modulus measurements at frequencies less than 0.1 rad/s. Therefore, for consistency the value of the storage modulus at 0.1 rad/s is used. A value of M_c (molar mass between effective cross-links) can be calculated on the basis of either

$$M_c = \frac{\rho RT}{G_e} \tag{10}$$

or

$$\frac{1}{M_c} = \frac{2}{M_n} + \frac{G_e}{\rho RT} \tag{11}$$

where ρ is the density of the polymer, G_e is the equilibrium modulus, T is the temperature, and M_n is the average overall molar mass of the whole chain. Equation 11 due to Flory[78] assumes that a COO^- group will not be located at the end of the chain and that each chain would have two dangling arms at its ends. Given our synthesis scheme, we will have a combination of chains without COO^- groups at both ends and chains with COO^- groups at both ends, and hence eq 10 serves as an upper bound and eq 11 a lower bound to the value of M_c in these ionomers. From the measured values of G_e and the overall molar mass of the chains, M_c can be estimated from either eq 10 or eq 11. For 11K-f1-Zn, eq 11 predicts a M_c of 10K and eq 10 predicts a M_c of 16K. Therefore, at least 70% (11K/16K) of ions form ionic triplets and consecutive ions along a chain form elastic strands. For simplicity, we have assumed in these calculations that the cation interaction with the backbone oxygen is weak and does not contribute to the elastic modulus. For the 11K-f1-Na, the numbers predicted are the same. This shows that once the equilibrium structure is reached, the nature of the cation has little influence on the equilibrium modulus achieved, though as we shall show in a subsequent paper the cation can influence the morphology of the equilibrium structure dramatically.

For 27K-f1-Zn, eq 11 predicts a M_c of 14K and eq 10 predicts a M_c of 27K. The lower value of M_c would imply 200% participation (27K/14K) of ions in ionic triplet formation, which is impossible. Rather, this low value of M_c reflects trapped entanglements. Because PDMS has an entanglement molecular weight of 10K, the 27K precursors can have entanglements trapped between the ionic physical cross-links. These trapped entanglements act as cross-links to enhance the modulus. Thus, the prediction of 100% (27K/27K) participation of ions from eq 10 also needs to be discounted for trapped entanglements. For 15K-f1-Na, eq 11 predicts a M_c value of 11K, again reflecting the contribution due to entanglements. Equation 10 predicts a M_c value of 20K. Thus, here too at least 75% (15K/20K) of the ions participate in ionic triplet formation.

Figure 14a shows the rheology of 11K-f1-Zn after 315 h at 150 °C and then cooling to 25 °C. The storage modulus is almost completely independent of frequency over many orders of magnitude, indicating the formation of a network with few structural defects that dissipate energy in this range of frequency. The rheology of 11K-f1-Na (Figure 14b) also shows a storage modulus independent of frequency. The value of the storage modulus of these almost-equilibrated samples is the same for the 11K-f1-Zn and 11K-f1-Na samples, though the kinetics to get to the equilibrium state are faster for sodium, a result that can be explained on the basis of the stronger ionic nature of sodium as compared to zinc. The value of the storage modulus decreases on cooling as expected for an elastomer.

Several theoretical frameworks have been proposed in the literature to capture the different relaxation time scales via the storage modulus and loss modulus in physically cross-linked systems.[79−81] Because time−temperature superposition is not

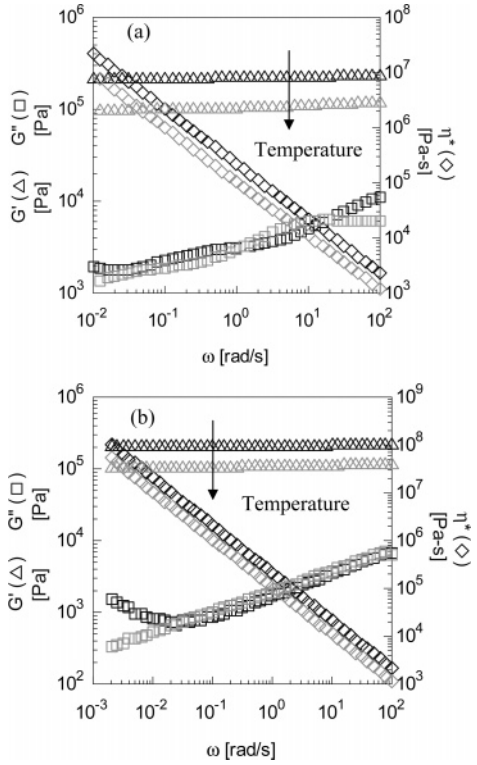

Figure 14. (a) G', G'', and η^* for 11K-f1-Zn after 315 h at 150 °C and after cooling to 25 °C. (b) G', G'', and η^* for 11K-f1-Na after 265 h at 150 °C and after cooling to 25 °C.

valid for our ionomers and we cannot obtain a master curve that extends from very high to very low frequencies, the average duration of an association and the longest relaxation time cannot be determined for our samples. This precludes any comparison with available models.

4. Conclusions

We have synthesized a series of associating poly(dimethylsiloxane) polymers containing interacting carboxylic acid or Zn/Na/Co carboxylate groups at regular intervals along the backbone. Our synthesis strategy allows for systematic control of the number of monomers between ions and the number of ions per chain. We find that the equilibrium state of these polymers in the melt is an elastic physical network formed as a result of cation−carboxyl anion interactions. In the case of zinc and cobalt, STEM results indicate a lack of aggregates of ionic triplets. We believe therefore that physical gel formation occurs via conversion of intramolecular linkages into intermolecular linkages. The gel time is governed by temperature, ion concentration, functionality, and the type of counterion. On the basis of the Arrhenius relationship that we observe for the gel time, we predict carboxylic acid containing PDMS polymers will form gels after years at room temperature whereas we predict and show some Zn carboxylate polymers form gels in a few months at room temperature. Critical gel exponent n and strength S along with t_{gel} are subject to competing influences of ion concentration and functionality for a given overall molar mass.

Acknowledgment. This work was supported by the National Science Foundation Polymers Program under Grant DMR-0349952. This work made use of the Cornell Center for Materials Research Shared Experimental Facilities supported through the National Science Foundation Materials Research Science and Engineering Centers program (Award DMR-0079992). We acknowledge Hansoo Kim and Karen Winey for the STEM results discussed here. Nozomi Ando and Sol Gruner are acknowledged for discussions regarding X-ray scattering. F. Escobedo and D. Bhawe are also acknowledged for useful discussions.

References and Notes

(1) Eisenberg, A.; Kim, J. S. *Introduction to Ionomers*; Wiley: New York, 1998; p 2.
(2) Jérôme, R.; Mazurek, M. In *Ionomers: Synthesis, Structure, Properties and Applications*; Tant, M. R., Mauritz, K. A., Wilkes, G. L., Eds.; Chapman & Hall: New York, 1997; pp 16−18.
(3) Horrion, J.; Jérôme, R.; Teyssié, P. *J. Polym. Sci., Part C: Polym. Lett.* **1986**, *24*, 69−76.
(4) Jérôme, R. *Telechelic Polymers: Synthesis and Applications*; Goethals, E. J., Ed.; CRC: Boca Raton, FL, 1989; Chapter 11.
(5) Jérôme, R.; Broze, G. *Rubber Chem. Technol.* **1985**, *58*, 223−242.
(6) Vanhoorne, P.; Jérôme, R. In *Ionomers: Characterizations, Theory and Applications*; Schlick, S., Ed.; CRC: Boca Raton, FL, 1996; Chapter 9.
(7) Mohajer, Y.; Bagrodia, S.; Wilkes, G. L.; Storey, R. F.; Kennedy, J. P. *J. Appl. Polym. Sci.* **1984**, *29*, 1943−1950.
(8) Hara, M.; Eisenberg, A.; Storey, R.; Kennedy, J. P. In *Columbic Interactions in Macromolecular Systems*; Eisenberg, A., Bailey, F. E., Eds.; ACS Symposium Series 302; American Chemical Society: Washington, DC, 1986; Chapter 14.
(9) Eisenberg, A.; Kim, J. S. *Introduction to Ionomers*; Wiley: New York, 1998; pp 214−233.
(10) Lee, D. C.; Register, R. A.; Yang, C. Z.; Cooper, S. L. *Macromolecules* **1988**, *21*, 1005−1008.
(11) Ding, Y. S.; Register, R. A.; Yang, C. Z.; Cooper, S. L. *Polymer* **1989**, *30*, 1204−1212.
(12) Register, R. A.; Yu, X.; Cooper, S. L. *Polym. Bull.* **1989**, *22*, 565−571.
(13) Visser, S. A.; Cooper, S. L. *Macromolecules* **1991**, *24*, 2576−2583.
(14) Mark, J. E. In *Silicon Based Polymer Science*: *A Comprehensive Resource*; Zeigler, J. M., Gordon Fearon, F. W., Eds.; American Chemical Society: Washington, DC, 1990; p 47.
(15) Patel, S.; Malone, S.; Cohen, C.; Gillmor, J.; Colby, R. *Macromolecules* **1992**, *25*, 5241−5251.
(16) Sivasailam, K.; Cohen, C. *J. Rheol.* **2000**, *44*, 897−915.
(17) Graessley, W. W. *Polymeric Liquids & Networks: Structure and Properties*: Garland Science: New York, 2004; Chapters 9 and 10.
(18) Boutevin, B.; Guida-Pietrasanta, F. In *Silicon-Containing Polymers*; Jones, R. G., Ando, W., Chojnowski, J., Eds.; Kluwer: Dordrecht, 2000; pp 79−112.
(19) Bindl, J.; Petersen, H.; Bachhuber, K.; Ott, M. U.S. Patent 5,504,233, 1996.
(20) Bachrach, A.; Zilkha, A. *Eur. Polym. J.* **1984**, *20*, 493−500.
(21) Abed-Ali, S. S.; Brisdon, B. J.; England, R. *Macromolecules* **1989**, *22*, 3969−3973.
(22) Boutevin, B.; Guida-Pietrasanta, F.; Ratsimihety, A. *J. Polym. Sci., Part A: Polym. Chem.* **2000**, *38*, 3722−3728.
(23) Fish, D.; Wu, E.; Khan, I. M.; Smid, J. *Polym. Prepr. (Am. Chem. Soc., Div. Polym. Chem.)* **1989**, *30*, 187−188.
(24) Fish, D.; Zhou, G.; Smid, J. *Polym. Prepr. (Am. Chem. Soc., Div. Polym. Chem.)* **1990**, *31*, 36−37.
(25) Zhandov, A. A.; Kashutina, E. A.; Shchegolikhina, O. I. *Polym. Sci. USSR* **1980**, *22*, 1699−1706.
(26) Shchegolikhina, O. I.; Vasil'ev, V. G.; Rogovina, L. Z.; Levin, V. Y.; Zhdanov, A. A.; Slonimskii, G. L. *Polym. Sci. USSR* **1991**, *22*, 2228−2235.
(27) Rogovia, L. Z.; Vasil'ev, V. G.; Papkov, V. S.; Shchegolikhina, O. I.; Slonimskii, G. L.; Zhdanov, A. A. *Macromol. Symp.* **1995**, *93*, 135−142.
(28) Vasil'ev, V. G.; Shchegolikhina, O. I.; Myagkov, R. A.; Rogovina, L. Z.; Zhdanov, A. A.; Papkov, V. S. *J. Polym. Sci., Ser. A* **1997**, *39*, 485−493.
(29) Blagodatskikh, I. V.; Shchegolikhina, O. I.; Larina, T. A.; Zhandov, A. A. *J. Polym. Sci., Ser. A* **1996**, *38*, 1239−1243.
(30) Ohyanagi, M.; Ikeda, K.; Sekine, Y. *Makromol. Chem., Rapid Commun.* **1983**, *4*, 795−799.
(31) Ohyanagi, M.; Kanai, H.; Katayama, Y.; Ikeda, K.; Sekine, Y. *Polym. Commun.* **1985**, *26*, 249−251.
(32) Katayama, Y.; Kato, T.; Ohyanagi, M.; Ikeda, K.; Sekine, Y. *Makromol. Chem., Rapid Commun.* **1986**, *7*, 465−470.
(33) Rajagopalan, P.; Wang, Z. Y.; Tsagaropoulos, G.; Risen, W. M. *J. Mol. Struct.* **1997**, *405*, 59−66.
(34) Klok, H.; Rebrov, E. A.; Muzafarov, A. M.; Michelberger, W.; Moller, M. *J. Polym. Sci., Part B: Polym. Phys.* **1999**, *37*, 485−495.

(35) Lee, C. L.; Johannson, O. K. *J. Polym. Sci., Polym. Chem. Ed.* **1976**, *14*, 729−742.
(36) Lee, C. L.; Marko, O. W.; Johannson, O. K. *J. Polym. Sci., Polym. Chem. Ed.* **1976**, *14*, 743−758.
(37) Lee, C. L.; Frye, C. L.; Johannson, O. K. *Polym. Prepr. (Am. Chem. Soc., Div. Polym. Chem.*) **1969**, *10*, 1361−1367.
(38) Lewis, L. N.; Carothers, T. W. U.S. Patent 5,550,272, 1996.
(39) Bryan, D. B.; Hall, R. F.; Holden, K. G.; Huffman, W. F.; Gleason, J. G. *J. Am. Chem. Soc.* **1977**, *99*, 2353−2355.
(40) Chandrasekaran, S.; Kluge, A. F.; Edwards, J. A. *J. Org. Chem.* **1977**, *42*, 3972−3974.
(41) Lim, K. T.; Webber, S. E.; Johnston, K. P. *Macromolecules* **1999**, *32*, 2811−2815.
(42) Strazzolini, P.; Dall'Arche, M. G.; Giumanini, A. G. *Tetrahedron Lett.* **1998**, *39*, 9255−9258.
(43) Blagodatskikh, I. V.; Sutkevich, M. V.; Sitnikova, N. L.; Churochkina, N. A.; Pryakhina, T. A.; Philippova, O. E.; Khokhlov, A. R. *J. Chromatogr. A* **2002**, *976*, 155−164.
(44) Brozoski, B. A.; Coleman, M. M.; Painter, P. C. *Macromolecules* **1984**, *17*, 230−234.
(45) Brozoski, B. A.; Painter, P. C.; Coleman, M. M. *Macromolecules* **1984**, *17*, 1591−1594.
(46) Batra, A. Ph.D. Thesis, Cornell University, Ithaca, NY, 2005.
(47) Richtering, H. W.; Gagnon, K. D.; Lenz, R. W.; Fuller, R. C.; Winter, H. H. *Macromolecules* **1992**, *25*, 2429−2433.
(48) Izuka, A.; Winter, H. H.; Hashimoto, T. *Macromolecules* **1994**, *27*, 6883−6888.
(49) Te Nijenhuis, K.; Winter, H. H. *Macromolecules* **1989**, *22*, 411−414.
(50) Madbouly, S. A.; Ougizawa, T. *J. Macromol. Sci., Part B: Phys.* **2004**, *B43*, 655−670.
(51) Rodriguez, R.; Alvarez-Lorenzo, C.; Concheiro, A. *J. Controlled Release* **2003**, *86*, 253−265.
(52) Fernandez, B.; Corcuera, M. A.; Marieta, C.; Mondragon, I. *Eur. Polym. J.* **2001**, *37*, 1863−1869.
(53) Stein, A. D.; Hoffmann, D. A.; Marcus, A. H.; Leezenberg, P. B.; Frank, C. W.; Fayer, M. D. *J. Phys. Chem.* **1992**, *96*, 5255−5263.
(54) Bhargarva, S.; Cooper, S. L. *Macromolecules* **1998**, *31*, 508−514.
(55) Welty, A.; Ooi, S.; Grady, B. *Macromolecules* **1999**, *32*, 2989−2995.
(56) Ishioka, T.; Shimizu, M.; Watanabe, I.; Kawauchi, S.; Harada, M. *Macromolecules* **2000**, *33*, 2722−2727.
(57) Muthukumar, M.; Winter, H. H. *Macromolecules* **1986**, *19*, 1286−1286.
(58) Muthukumar, M. *Macromolecules* **1989**, *22*, 4658−4660.
(59) Takenaka, M.; Kobayashi, T.; Hashimoto, T.; Takahashi, M. *Phys. Rev. E* **2002**, *65*, 041401-1−041401-7.
(60) Pogodina, N. V.; Winter, H. H. *Macromolecules* **1998**, *31*, 8164−8172.
(61) Lin, Y. G.; Mallin, D. T.; Chien, J. C. W.; Winter, H. H. *Macromolecules* **1991**, *24*, 850−854.
(62) Scanlan, J. C.; Winter, H. H. *Macromolecules* **1991**, *24*, 47−54.
(63) Izuka, A.; Winter, H. H.; Hashimoto, T. *Macromolecules* **1992**, *25*, 2422−2428.
(64) Batra, A.; Cohen, C.; Kim, H.; Winey, K. I.; Ando, N.; Gruner, S. *Macromolecules*, submitted.
(65) Chu, B. In *Ionomers: Characterizations, Theory and Applications*; Schlick, S., Ed.; CRC: Boca Raton, FL, 1996; Chapter 3.
(66) Register, R. A.; Cooper, S. L. *Macromolecules* **1990**, *23*, 310−317.
(67) Register, R. A.; Prud'homme, R. K. In *Ionomers: Synthesis, Structure, Properties and Applications*; Tant, M. R., Mauritz, K. A., Wilkes, G. L., Eds.; Chapman & Hall: New York, 1997; pp 208−260.
(68) Brown, S. B.; Yates, J. B. W. O. Patent 8,700,520, 1987.
(69) Coleman, M. M.; Lee, J. Y.; Painter, P. C. *Macromolecules* **1990**, *23*, 2339−2345.
(70) Kutsumizu, S.; Nakamura, M.; Yano, S. *Macromolecules* **2001**, *34*, 3033−3040.
(71) Vasil'ev, V. G.; Rogovina, L. Z.; Slonimskii, G. L.; Papkov, V. S.; Schegolikhina, O. I.; Zhdanov, A. A. *J. Polym. Sci., Ser. A* **1995**, *37*, 174−178.
(72) Eisenberg, A. *Macromolecules* **1971**, *4*, 125−128.
(73) Bagrodia, S.; Wilkes, G. L. *Polym. Bull. (Berlin)* **1984**, *12*, 389−392.
(74) Bagrodia, S.; Wilkes, G. L.; Kennedy, J. P. *Polym. Eng. Sci.* **1986**, *26*, 662.
(75) Tant, M. R.; Venkateshwaran, L. N.; Song, J. H.; Subramanian, R.; Wilkes, G. L.; Charlier, P.; Jérôme, R. *Polymer* **1992**, *33*, 1347−1358.
(76) Horrion, J.; Jérôme, R.; Teyssie, P.; Williams, C. E. *Polymer* **1988**, *29*, 1203−1210.
(77) Han, K.; Williams, H. L. *J. Appl. Polym. Sci.* **1991**, *42*, 1845−1859.
(78) Flory, P. J. *Principles of Polymer Chemistry*; Cornell University Press: Ithaca, NY, 1953.
(79) Tanaka, F.; Edwards, S. F. *Macromolecules* **1992**, *25*, 1516−1523.
(80) Leibler, L.; Rubinstein, M.; Colby, R. H. *Macromolecules* **1991**, *24*, 4701−4707.
(81) Jongschaap, R. J. J.; Wientjes, R. H. W.; Duits, M. H. G.; Mellema, J. *Macromolecules* **2001**, *34*, 1031−1038.

MA051418Q